Journal of Catalysis **186,** 442–457 (1999)
Article ID jcat.1999.2570, available online at http://www.idealibrary.com on IDEAL®

An Investigation of the Al–Sb–V–W–Oxide System for Propane Ammoxidation

Jerker Nilsson,* Angel R. Landa-Cánovas,† Staffan Hansen,‡ and Arne Andersson*,[1]

*Department of Chemical Engineering II (Chemical Technology), University of Lund, Chemical Center, P.O. Box 124, SE-221 00 Lund, Sweden; †Centro de Microscopia Electronica, Universidad Complutense de Madrid, Ciudad Universitaria, E-28040 Madrid, Spain; and ‡National Center for HREM, Inorganic Chemistry 2, University of Lund, Chemical Center, P.O. Box 124, SE-221 00 Lund, Sweden

Received March 24, 1999; revised May 17, 1999; accepted May 17, 1999

Al–Sb–V–W–oxide catalysts were prepared and used for propane ammoxidation to give acrylonitrile. The preparations were characterized, both as freshly prepared and after use in propane ammoxidation, using XRD, XPS, Raman spectroscopy, and transmission electron microscopy together with electron diffraction and X-ray microanalysis. Activity tests of the freshly prepared samples reveal a remarkable activation behaviour with time-on-stream under influence from the reaction medium. During the first 15–50 h on-stream, a considerable increase in the activity and the selectivity to acrylonitrile is observed in parallel with a decrease in the selectivity to waste products. The duration of the activation period depends on the W-content and increases with increase of the latter. Characterization with TEM, electron diffraction, and X-ray microanalysis show that the activation of the catalyst precursor under reaction conditions results in the formation of an $\approx$Sb(V, W)O_4 phase of rutile-type, which is active and selective to acrylonitrile formation. The aluminum in the catalysts is present in form of δ-Al_2O_3, which serves as a catalyst support. Analysis of the catalysts and their precursors with XPS shows coverage of the alumina surface with oxides with Sb, V, and W, and the Raman spectra show the presence of tetrahedral and octahedral tungsten oxide species being attached to the alumina surface. Both XPS and X-ray microanalysis results indicate that the surfaces and the external layers of the precursors are enriched with antimony. Activity test of an Al–Sb–V–W–oxide catalyst with Sb : V : W = 5 : 1 : 2 and 50 wt% Al_2O_3, using a feed which is stoichiometric with respect to acrylonitrile formation, shows that the selectivity to acrylonitrile is 48% at 77% propane conversion, corresponding to a yield of 37%. Comparison with Sb–V–oxide and Al–Sb–V–oxide preparations reveals a substantial improvement of the catalytic properties with the addition of Al and W to Sb–V–oxide.

Key Words: **propane; ammoxidation; acrylonitrile formation; Al–Sb–V–W–oxide catalysts; catalyst characterization; XRD; XPS; Raman spectroscopy; transmission electron microscopy; electron diffraction; X-ray microanalysis.**

INTRODUCTION

There is presently worldwide interest in developing heterogeneous catalysts that are active for the partial oxidation of alkanes, enabling the replacement of the corresponding olefins as feedstocks in chemicals production (1). A driving force for this trend is the competition that exists for light olefins between various sectors, including partial oxidation, polymerization, and refinery processes. As a result, in various parts of the world there is a considerable difference in price between C_2–C_4 olefins and the corresponding alkanes, which is in favor of the alkanes. Partial oxidation of an alkane is already in practice for the manufacture of maleic anhydride, where butane oxidation has replaced older technologies using butene or benzene as feedstock (2). Currently, BP/SOHIO is active in developing a process for the direct manufacture of acrylonitrile from propane, as an alternative to their well-known ammoxidation process starting from propylene (3). BP has announced (29 May 1997) the successful operation of a first-stage demonstration plant (4). According to BP, the propane process offers 20% lower production costs compared to the route from propylene. Moreover, on an overall cost basis, BP claims that the one-step propane process is advantaged over two-step facilities which in a first step generate their propylene feedstock via propane dehydrogenation.

For propane ammoxidation different types of catalysts have been reported to be active, such as Bi–Mo–V scheelites (5–7), rutiles with Sb, V, W, and Al as key elements (8–10), and Mo–V mixed oxide modified with Nb and Te (11). A comparison of the activity data which has been reported for the different catalyst systems indicate that the Al–Sb–V–W–O rutile system is a most promising catalyst candidate, which gives a yield of ~40% acrylonitrile at ~70% propane conversion (8). However, the Al–Sb–V–W–oxide system is complex. According to the patents (8), $\approx SbVO_4$ (12, 13) is a crucial catalyst component, and the presence in the finished catalyst of excess antimony oxide

[1] Correspondence should be sent to Dr. Arne Andersson, Dept. of Chemical Engineering II, Chemical Center, P.O. Box 124, S-221 00 Lund, Sweden. Fax: +(46-46)149156. E-mail: Arne.Andersson@chemeng.lth.se.

0021-9517/99 $30.00

(Sb : V = 3–7) as Sb_2O_4 results in superior catalytic performance. Aluminum in the form of alumina was considered a catalyst support, while tungsten was considered an element of the active material. The data given in the patents (8) show a remarkable successive improvement in the catalytic properties when excess Sb, Al, and W, respectively, are added to the Sb–V–oxide. Examples show that the yield to acrylonitrile is about 4% over $VSbO_x/SiO_2$ and 10–12% over both unsupported and silica-supported VSb_5O_x. The yield is higher, 20–30%, for VSb_5O_x on an Al-rich support (80 wt% alumina and 20 wt% silica). When tungsten is added the yield to acrylonitrile is further improved and reaches 25–40% for VSb_5WO_x/Al_2O_3–SiO_2. Data which are available in the literature confirm the trend (9, 10, 14–17).

Our previous work has shown that there are significant differences between the Sb–V–O and Al–Sb–V–O systems concerning the composition and the catalytic performance of the active rutile phase. We have reported (18) that heating equimolar mixtures of Sb_2O_3 and V_2O_5 at 800°C in flowing gas with varying O_2/N_2 ratios produces a continuos nonstoichiometric series of rutile type with cation vacancies (□), i.e., $Sb_{0.9}V_{0.9+x}\square_{0.2-x}O_4$ ($0 < x < 0.2$) and varying amounts of α-Sb_2O_4. The phase which is obtained in air has the approximate composition $Sb_{0.92}V_{0.92}O_4$, or $Sb(V)_{0.92}V(III)_{0.28}V(IV)_{0.64}\square_{0.16}O_4$ (19), and it is also formed in catalysts prepared by heating a slurry of Sb_2O_3 and NH_4VO_3 in water followed by calcination at 610°C. We have identified the active phase in the Sb–V–O system as being $\approx SbVO_4$ enriched with antimony at the surface (14, 15, 20). The antimony-enriched $\approx SbVO_4$ is considerably more selective than the pure phase to acrylonitrile. The spreading of antimony from the excess α-Sb_2O_4 to the surface of $\approx SbVO_4$ occurs both during the preparation of the catalyst and to some extent during propane ammoxidation (20). For catalyst synthesis in the Al–Sb–V–O system there is quite a different reason for using an Sb : V ratio greater than one. In this system we have identified $Al_{1-x}SbV_xO_4$ ($0 < x < 0.5$), which presents a trirutile-type superlattice, as being the most selective phase towards acrylonitrile formation (16). Moreover, formation of $Al_{1-x}SbV_xO_4$ was not observed starting from the phase composition, but required an excess of alumina. Without alumina in excess, $\approx SbVO_4$ was formed. Besides being an element in the active phase, aluminum also acts as a support in form of δ-Al_2O_3.

Concerning the Al–Sb–V–W–O system, we have recently reported the formation of a phase with the average composition $Al_{0.1}Sb_{0.8}V_{0.7}W_{0.4}O_4$ (17), which was found to be present in an ammoxidation catalyst with the nominal composition Al : Sb : V : W = 21 : 5 : 1 : 1. In the present paper we report a more detailed characterization of this important catalyst system, where we have studied catalysts with different V : W ratios for propane ammoxidation.

EXPERIMENTAL

Preparation of Samples

The Al–Sb–V–W–oxide catalysts were prepared by the following slurry method. Sb_2O_3 (Merck, p.a.) was dispersed in water and a hot aqueous solution of NH_4VO_3 (Merck, p.a.) was added as well as $Al(OH)_3$ (Riedel-de-Haën, p.a.). The mixture was refluxed for 17 h. An aqueous solution of $(NH_4)_6W_{12}(OH)_2O_{38}$ (Strem Chemicals, p.a.) was then added under stirring and heating for a few hours. The resulting mixture was first dried at 110–120°C and then precalcined in air for 5 h at 350°C. After screening, the solid material was calcined twice, first in air for 3 h at 530°C and then eventually in air for another 2 h at 610°C. When only two of the elements Sb, V, and W are included in the preparation, the same procedure was principally used with the necessary modification.

For comparative purposes, three other samples were prepared. A sample of the pure phase $Sb_{0.9}V_{0.9}O_4$ (18, 19) was obtained by heating an equimolar mixture of V_2O_5 (Riedel-de-Haën, p.a.) and Sb_2O_3 in air at 800°C for 18 h. An Sb–V–O sample containing α-Sb_2O_4 and $Sb_{0.9}V_{0.9}O_4$ and with the nominal atomic ratio Sb : V = 2 : 1 was prepared from a slurry of Sb_2O_3 in water solution with NH_4VO_3, which was heated under reflux before drying and final calcination at 610°C (14, 15). WO_3 was prepared by calcination of $(NH_4)_6W_{12}(OH)_2O_{38}$ at 800°C for 8 h in air.

The notations which are used for the catalyst samples are given in Table 1.

Characterization of Samples

For X-ray powder diffraction (XRD), the samples were crushed and mounted on adhesive tape. Films were recorded using a Guinier–Hägg focusing camera with Cu $K\alpha_1$ radiation (wavelength 1.54056 Å) and with Si as internal standard (cubic cell constant 5.43088 Å).

Quantitative elemental analysis was carried out in a transmission electron microscope with a field emission

TABLE 1

Notation, Composition, and Specific Surface Area of Catalyst Samples

Catalyst notation	Atomic ratio Sb : V : W	Al_2O_3 support (wt%)	Specific surface area (m^2/g)
Sb5V1–Al	5 : 1 : 0	50	128
Sb5V1W0.5–Al	5 : 1 : 0.5	50	128
Sb5V1W1–Al	5 : 1 : 1	50	116
Sb5V1W2–Al	5 : 1 : 2	50	104
Sb5V1W5–Al	5 : 1 : 5	50	114
Sb5W1–Al	5 : 0 : 1	50	123
Sb2V1	2 : 1 : 0	Unsupported	4
$Sb_{0.9}V_{0.9}O_4$, pure	1 : 1 : 0	Unsupported	2
WO_3, pure		Unsupported	3

electron gun, Philips CM200 FEG (acceleration potential 200 kV and spherical aberration lens constant 1.2 mm). The diameter of the electron beam was 1 nm, and the emitted X-ray radiation was registered using an EDAX detector with super-ultra-thin window. The energy resolution was 134.2 eV.

Identification and imaging of the phases present in the samples were performed in a transmission electron microscope, JEM-2000FX, which was operated at an acceleration voltage of 200 kV and fitted with an energy dispersive X-ray analysis system, Link AN10000. The phases were identified by a combination of selected area electron diffraction, which was recorded the crystal was tilted in different orientations, and qualitative elemental analysis.

BET surface areas were determined with a Micromeritics Flowsorb 2300 instrument, applying adsorption of N_2 at liquid N_2 temperature. The samples were degassed at 350°C. Specific surface areas of the samples which were used as catalysts are included in Table 1.

Raman measurements were performed with a Bruker IFS 66 FTIR spectrometer equipped with an FRA 106 Raman device. A low power diode pumped Nd:YAG laser with an excitation line at 1046 nm and a liquid nitrogen cooled germanium diode detector were used. Measurements were carried out under ambient conditions. The laser power was 50 mW and the resolution was 4 cm^{-1}. Backscattering at 180° was measured and 1000 scans were averaged.

XPS measurements were performed with a Kratos XSAM 800 instrument using Mg $K\alpha$ X-ray radiation (1253.6 eV). The anode was operated at an accelerating voltage of 13 kV and a current of 19 mA, and the pass energy was 80 eV at high magnification. The residual pressure inside the spectrometer was 10^{-8} Torr or lower. Measurements were performed on ground samples, which were attached to the sample holder with double-sided tape. For the samples with aluminum, charging effects were corrected for by adjusting the Al 2*s* signal to a position of 119.4 eV, otherwise the C 1*s* signal was set to a position of 285.0 eV. For quantitative purposes instrumental sensitivity factors were used together with linear base lines.

Activity Measurements

The activity measurements were performed using an isothermal plug-flow reactor made from glass. Conversion and selectivities were studied varying the amount of catalyst at constant flow rate. A fraction of catalyst particles with diameters in the range 0.150–0.425 mm was used. Dilution of the catalyst samples with quartz grains was necessary to have isothermal conditions. Dead volumes were reduced using glass beads, and hot zones in the tubing between the reactor and the analysis equipment were avoided to have negligible contribution from homogeneous conversion. A total flow of 70 ml (STP)/min was passed over 75–3300 mg of catalyst, corresponding to a space velocity (WHSV) in the range 56000–1300 ml/(h g). The reactor temperature was 480°C, and the composition of the feed expressed as the mole ratio propane/ammonia/oxygen/water vapor/nitrogen was 2:2:4:1:5, corresponding to the stoichiometric ratio between propane, oxygen, and ammonia for forming acrylonitrile. Propane and the products propylene, acrylonitrile, acetonitrile, ethylene, methane, CO, and CO_2 were analyzed on a GC which was equipped with a Porapak Q column, a sample valve, an FID detector, and a methaniser for analysis of the carbon oxides. Analyses of ammonia conversion and formation of HCN were performed using titrimetric methods (21). It was verified that the carbon balance was complete.

RESULTS

Activation Behaviour of Al–Sb–V–W–O Catalysts

As we have reported for Sb5V1–Al (17), neither Sb5W1–Al, nor the pure WO_3 showed any activation period in addition to the normal and very short transient behaviour during start-up of the reactor system. After the first few minutes on stream there was no trend for these samples, at least not during the first 20 h, indicating any change with time of the catalytic data. On the contrary, all of the catalysts containing antimony, vanadium, and tungsten, i.e., Sb5V1W0.5–Al, Sb5V1W1–Al, Sb5V1W2–Al, and Sb5V1W5–Al, showed a remarkable activation behaviour. This is illustrated in Fig. 1

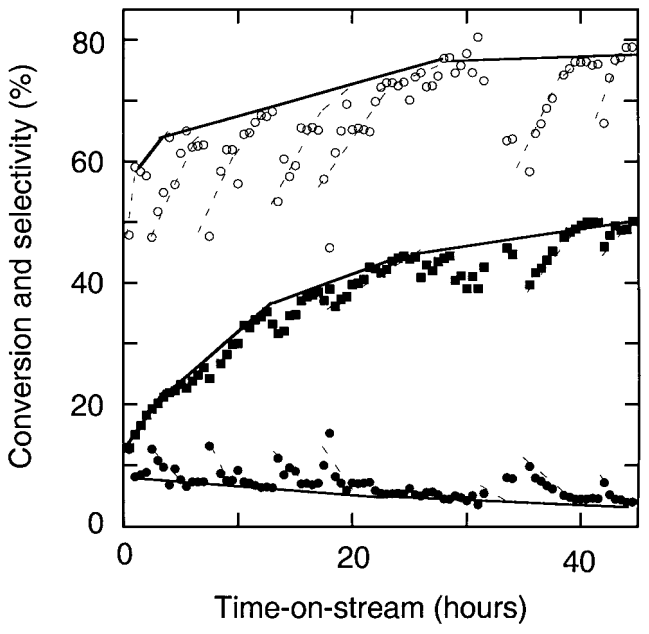

FIG. 1. Propane conversion (○) and selectivity to propylene (●) and acrylonitrile (■) over Sb5V1W2–Al as a function of time-on-stream in propane ammoxidation at 480°C. The dashed curves show the short-term reactivation occuring at the daily start-up of the reactor system. The experiment was run for 6 h for 7 days at a space velocity (WHSV) of 3000 ml/(h g).

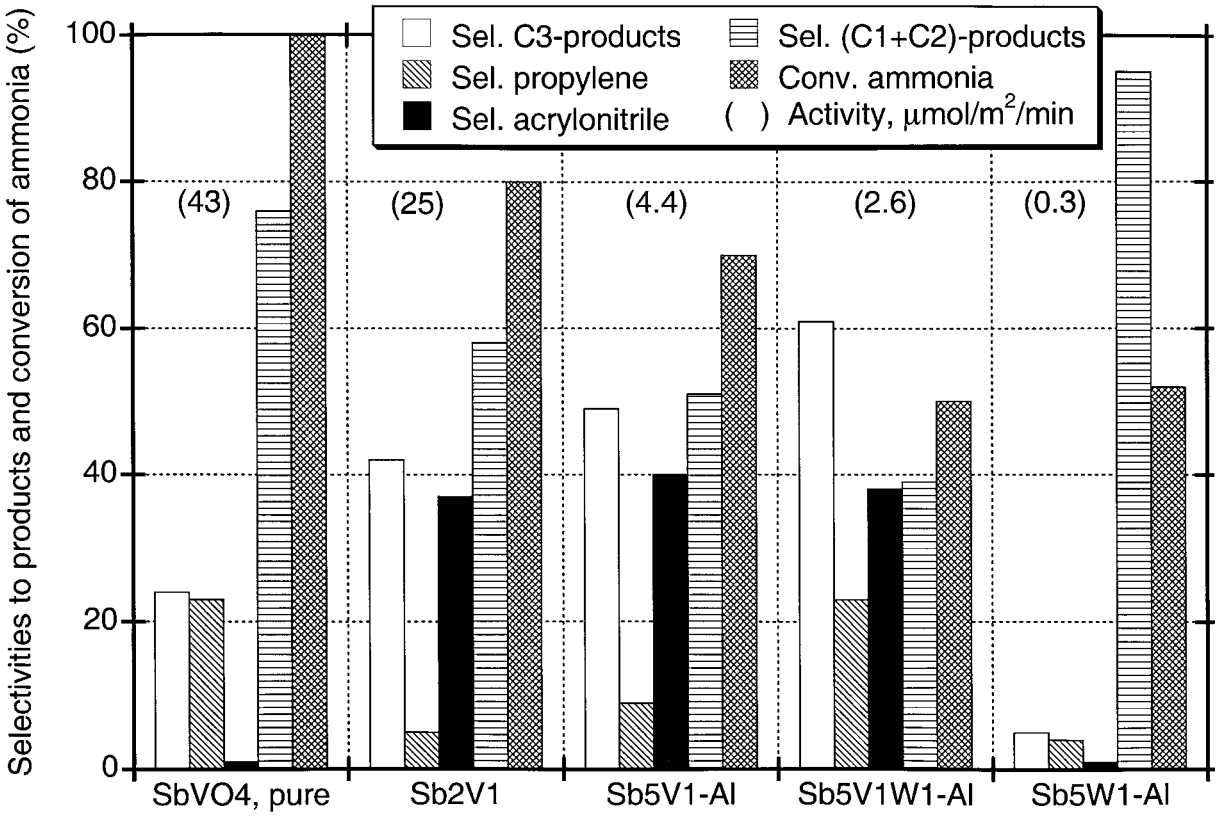

FIG. 2. Product selectivities and ammonia conversion in propane ammoxidation at 480°C and ~30% propane conversion over ≈$SbVO_4$, Sb2V1, Sb5V1–Al, Sb5V1W1–Al, and Sb5W1–Al (notations as in Table 1). The data are at 25% propane conversion for ≈$SbVO_4$ and at 30% propane conversion for the other samples. Activities, in μmol of propane conversion/m^2/min, are given in the figure within brackets.

with data for Sb5V1W2–Al. It is clearly seen from the figure that not only the activity but also the selectivity to acrylonitrile increases with time-on-stream. The activation process continues for at least a few days. Since we were unable to run the system during the night, the curves in Fig. 1 show in addition to the long-term activation also a daily short-term reactivation, which obviously is related to the cooling down of the reactor. Figure 1 shows that the conversion increases from ~58 to ~78% during the first 40 h on stream, and concurrently the selectivity to acrylonitrile increases from 12 to 50%. The substantial increase in the selectivity to acrylonitrile, however, is not balanced by a corresponding decrease of the selectivity to propylene, which only decreases from about 9 to 4%. Instead, the activation process was found to result in decreased waste formation and, especially, of carbon oxides.

Comparison of the activation behaviours of the Al–Sb–V–W–oxide catalysts showed a general trend, namely, that the long-term activation period increases with increase in the tungsten content of the catalyst. For similar series the activation period increases from about 15 h for Sb5V1W0.5–Al and Sb5V1W1–Al, see Ref. (17), to 40 and 50 h for Sb5V1W2–Al and Sb5V1W5–Al, respectively.

Propane Ammoxidation

Figure 2 gives a comparison of catalytic data for propane ammoxidation over a series of catalysts. In the figure the selectivities to the various products and the ammonia conversion are compared at 25–30% propane conversion. The results show that the pure ≈$SbVO_4$ phase has low selectivity to the C_3-products propylene and acrylonitrile. Over this catalyst mainly carbon oxides are formed and the ammonia is degraded to give nitrogen. Comparison of the data for ≈$SbVO_4$ with the corresponding data for Sb2V1, Sb5V1–Al, and Sb5V1W1–Al shows that the selectivity to the C_3-products, and especially to acrylonitrile, is substantially improved when the Sb : V atomic ratio is greater than one and also with the addition to the catalyst of aluminum and tungsten. Thus, at 30% propane conversion the selectivity to the C_3-products increases in the sequence ≈$SbVO_4$ < Sb2V1 < Sb5V1–Al < Sb5V1W1–Al. In parallel to the increase in the selectivity to C_3-products there is a decrease in the ammonia conversion. The catalytic data in Fig. 2 clearly demonstrate the better catalytic properties of the Al–Sb–V–W–oxide system as compared to the Al–Sb–V–O and Sb–V–O subsystems. Moreover, comparison

of the data for Sb5W1–Al with those for the catalysts containing vanadium evidences that vanadium is a cardinal element in the catalyst for obtaining selective conversion of propane to propylene and acrylonitrile. Over Sb5W1–Al mainly degradation to carbon oxides occurs, but there is also some conversion (6%) to acetonitrile. Comparison of the activities shows a decrease in the activity with decrease of the vanadium content of the catalyst. The activity of the pure WO_3 was very low. As we previously have reported for the pure V_2O_5 and Sb_2O_4 phases (16), the WO_3 phase was unable to convert the formed propylene further to acrylonitrile. When the conversion over WO_3 was increased from 3 to 9%, the selectivity to propylene decreased from 72 to 43% simultaneously as the selectivity to acrylonitrile increased from 4 to only 7%.

In Fig. 3 are selectivities to products and the ammonia conversion compared at 60% propane conversion for a series of catalysts with various contents of tungsten. The data show that the selectivity to acrylonitrile, as well as the sum of the selectivities to propylene and acrylonitrile both, passes through a maximum with increase in the tungsten content of the catalyst. The best performance is shown by Sb5V1W1–Al and Sb5V1W2–Al. For both samples the selectivity to C_3-products and acrylonitrile are about 57 and 47%, respectively. The maximum in the selectivity to C_3-products is associated with a corresponding minimum in the selectivity to carbon oxide formation. Although the error bar is around $\pm 2\%$ for selectivities in the 40–60% range, the maximum is confirmed by comparing the data for Sb5V1W1–Al and Sb5W1-Al in Fig. 2. Moreover, Fig. 3 shows that the selectivity to acetonitrile is higher over the catalysts with tungsten than is obtainable over Sb5V1–Al, ~16 and 4%, respectively. The selectivity to HCN is small over all samples and decreases from 8 to 4% with increase in the tungsten content. No clear trend is observed for the ammonia conversion. It is generally in the range 80–90%, except for being about 70% over Sb5V1W5–Al. The activity data, which are inserted in the figure, point to a decrease in the activity when the content of tungsten is increased.

The performance of Sb5V1W2–Al as a function of the propane conversion is compared in Fig. 4 with the performances of Sb5V1–Al and Sb2V1. It is seen for all catalysts that the selectivity to propylene decreases with increasing conversion of propane, simultaneously as the selectivity

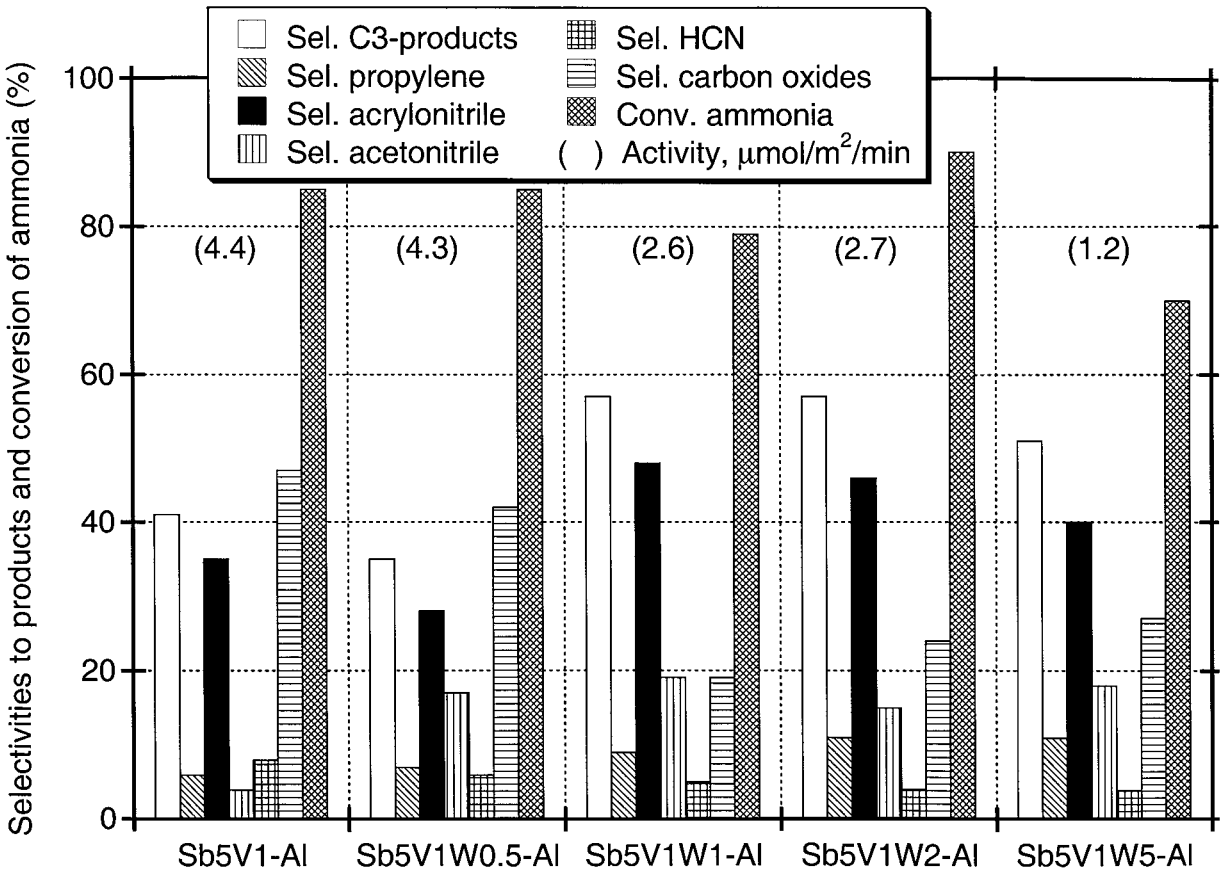

FIG. 3. Product selectivities and ammonia conversion in propane ammoxidation at 480°C and 60% propane conversion over a series of catalysts with varying tungsten content. For catalyst notations, see Table 1. Activities, in μmol of propane conversion/m^2/min, are given in the figure within brackets.

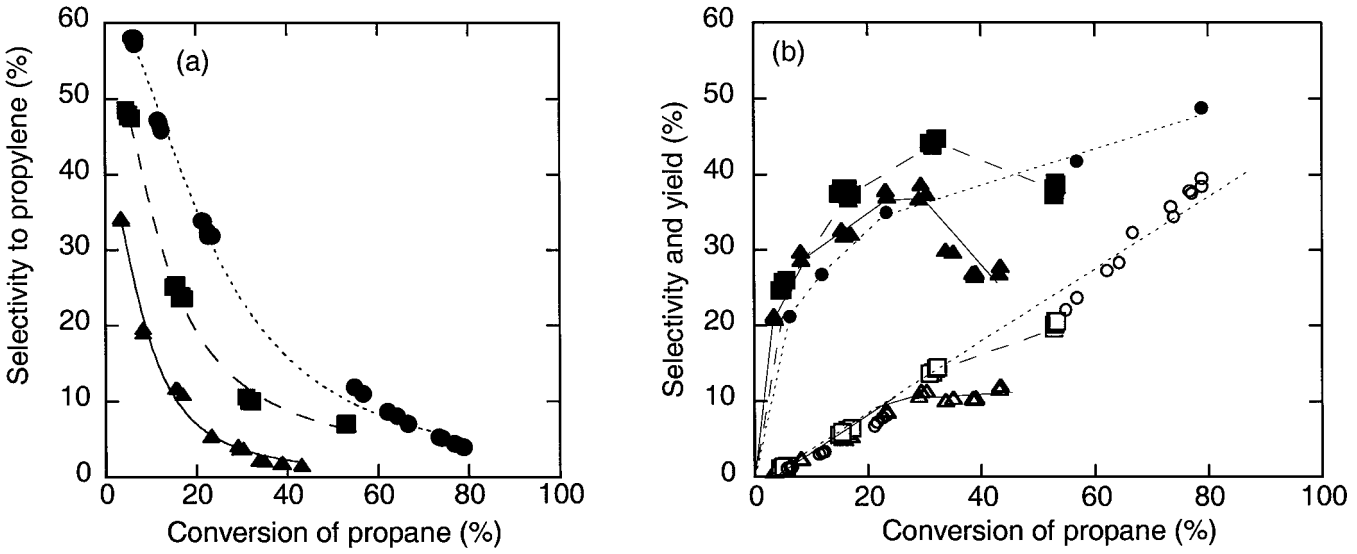

FIG. 4. Comparison of the propane ammoxidation at 480°C over Sb2V1, Sb5V1–Al, and Sb5V1W2–Al (notations as in Table 1) as a function of propane conversion. (a) The selectivity to propylene over Sb2V1 (▲), Sb5V1–Al (■), and Sb5V1W2–Al (●). (b) The selectivity to acrylonitrile over Sb2V1 (▲), Sb5V1–Al (■), and Sb5V1W2–Al (●), and the yield to acrylonitrile over Sb2V1 (△), Sb5V1–Al (□), and Sb5V1W2–Al (○).

to acrylonitrile increases and for Sb2V1 and Sb5V1–Al passes through a maximum. For Sb2V1, Sb5V1–Al, and Sb5V1W2–Al the highest selectivity to acrylonitrile is 37, 45, and 48%, respectively, and is obtained at 25, 30, and 77%, propane conversion, respectively. Consequently, the yield to acrylonitrile increases with the conversion of propane and reaches at most 11, 20, and 37% for Sb2V1, Sb5V1–Al, and Sb5V1W2–Al, respectively. The performance of Sb5V1W1–Al was very similar to that of Sb5V1W2–Al and the highest yield to acrylonitrile, 37%, was obtained at 80% propane conversion (17). Under the present conditions using a feed which is stoichiometric with regard to acrylonitrile formation, the yield is limited by the almost complete consumption of oxygen and ammonia.

Catalyst Characterisation

X-ray diffraction. The result of powder X-ray analyses of the prepared samples are collected in Table 2. All samples with aluminum were largely X-ray amorphous, but showed lines from crystalline α-Sb_2O_4. Except for Sb5V1W0.5–Al showing no diffraction lines from WO_3, the diffraction patterns of the other samples with Al, Sb, V, and W showed a few lines from monoclinic WO_3. As the phase pure WO_3 sample, Sb5W1–Al gave reflections from triclinic WO_3. Comparing the X-ray analyses of freshly prepared and used samples showed no qualitative difference in phase composition.

X-ray photoelectron spectroscopy. In Table 3 the nominal metal compositions of the catalysts with alumina are compared with the corresponding surface compositions as measured by XPS before and after use in propane ammoxidation. Comparison shows that the Al content determined by XPS is considerably less than the nominal value, while the corresponding XPS analyses for Sb and W show enrichment of these elements. The data for V are somewhat scattered, but for the samples with W the surface concentration of V is generally higher than the nominal value.

Comparison of the XPS analyses for fresh samples with the used samples reveals that there is a considerable decrease in the surface content of Sb upon use in propane ammoxidation, while the V, W, and Al contents are increased.

The Sb $3d_{3/2}$, V $2p_{3/2}$, W $4d_{5/2}$, and Al 2*s* binding energies for the catalysts are collected in Table 4. The binding energy for Sb $3d_{3/2}$ is in the range 540.1–540.8 eV and the values for V $2p_{3/2}$ and W $4d_{5/2}$ are in the range 516.0–517.0 eV and

TABLE 2

Phases Identified by Powder X-Ray Diffraction

Sample	Phases[a]
Sb5V1–Al	α-Sb_2O_4
Sb5V1W0.5–Al	α-Sb_2O_4
Sb5V1W1–Al	α-Sb_2O_4; WO_3 (monoclinic)
Sb5V1W2–Al	α-Sb_2O_4; WO_3 (monoclinic)
Sb5V1W5–Al	α-Sb_2O_4; WO_3 (monoclinic)
Sb5W1–Al	α-Sb_2O_4, WO_3 (triclinic)
Sb2V1	α-Sb_2O_4; $Sb_{0.9}V_{0.9}O_4$
$Sb_{0.9}V_{0.9}O_4$, pure	$Sb_{0.9}V_{0.9}O_4$
WO_3, pure	WO_3 (triclinic)

[a] The phases were identified considering the references as follows: α-Sb_2O_4, JCPDS-file 11-694, Ref. (22); monoclinic WO_3, JCPDS-file 24-747, Ref. (22); triclinic WO_3, JCPDS-file 20-1323, Ref. (22); and $Sb_{0.9}V_{0.9}O_4$, Ref. (19).

TABLE 3

Nominal Metal Composition of Catalysts and Corresponding Surface Composition as Determined by XPS

Catalyst	Sb-content (at%)	V-content (at%)	W-content (at%)	Al-content (at%)
Sb5V1–Al				
Nominal	21.7	4.3	0.0	73.9
Fresh	53.0	3.0	0.0	44.0
Used	43.9	4.1	0.0	51.9
Sb5V1W0.5–Al				
Nominal	19.6	3.9	2.0	74.5
Fresh	73.5	6.0	7.5	13.0
Used	51.8	7.9	9.5	30.7
Sb5V1W1–Al				
Nominal	17.9	3.6	3.6	75.0
Fresh	52.7	3.1	10.5	33.7
Used	40.2	9.8	17.7	32.3
Sb5V1W2–Al				
Nominal	14.7	2.9	5.9	76.5
Fresh	48.3	13.7	11.1	26.9
Used	33.0	18.8	16.9	31.3
Sb5V1W5–Al				
Nominal	10.0	2.0	10.0	78.0
Fresh	40.1	6.3	12.1	41.4
Used	21.4	7.4	14.6	56.6

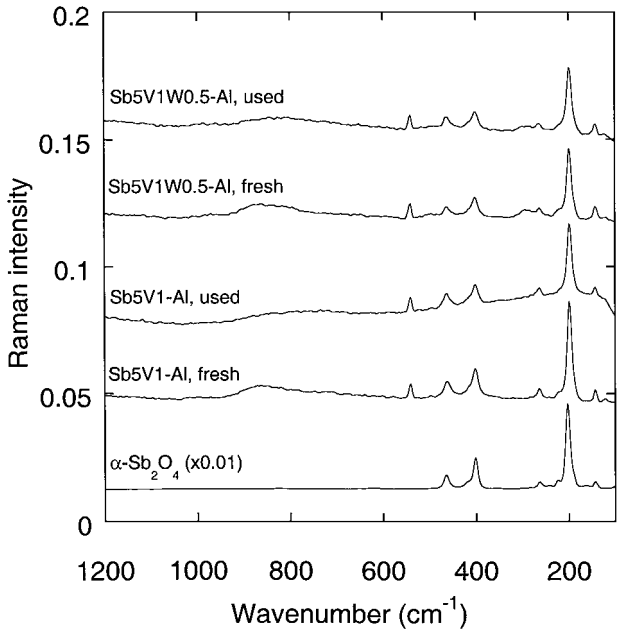

FIG. 5. Raman spectra of α-Sb_2O_4, and of Sb5V1–Al and Sb5V1W0.5–Al before and after use in propane ammoxidation. The small peak at 540 cm^{-1} is an instrumental artefact peak, which can be used for quantitative comparisons.

245.9–247.9 eV, respectively. The V $2p_{3/2}$ binding energy is 517.1 eV for V_2O_5 and 516.1 eV for VO_2. Sb_2O_5 has a Sb $3d_{3/2}$ binding energy of 540.3 eV and the corresponding value for Sb_2O_3 is 539.9 eV. WO_3 shows a W $4d_{5/2}$ binding energy of 247.7 eV.

Raman spectroscopy. Figure 5 shows the Raman spectra recorded for Sb5V1–Al and Sb5V1W0.5–Al before and after use in propane ammoxidation together with the spectrum of α-Sb_2O_4. Comparison of the spectra shows that in the region below 500 cm^{-1} there are predominantly bands from α-Sb_2O_4 in the catalyst spectra. Moreover, the intensity of the α-Sb_2O_4 bands is somewhat smaller after use of the catalysts in ammoxidation. In the region above 500 cm^{-1} the fresh Sb5V1–Al and Sb5V1W0.5–Al samples show a weak and broad feature around 870 cm^{-1}, which is almost absent in the spectra of the used samples.

When the tungsten content is further increased additional Raman bands appear as shown in Fig. 6. For Sb5V1W1–Al and Sb5V1W2–Al these bands are at 972, 870 (shoulder), and 807 cm^{-1}, and also a broad band appears at 684 cm^{-1}. All these bands increase in intensity with the W content, and also they become more intense after use of the samples in propane ammoxidation. Additionally, bands from α-Sb_2O_4 are present in the region below 500 cm^{-1}, and the intensity of these bands is smaller for the used samples than for the freshly prepared samples. The same Raman bands are apparent in the two spectra for Sb5V1W5–Al in Fig. 7, although the intensity of the bands in the region above 500 cm^{-1} hardly increases with use in ammoxidation. For Sb5W1–Al, which has no vanadium, the spectral features in Fig. 7 are different. Besides bands from α-Sb_2O_4, a broad band is seen around 943 cm^{-1} and there are also

TABLE 4

XPS Binding Energy Data for Catalysts and Some Reference Compounds

Catalyst	Sb $3d_{3/2}$ (eV)	V $2p_{3/2}$ (eV)	W $4d_{5/2}$ (eV)	Al 2*s* (eV)
Sb5V1–Al				
Fresh	540.2	516.3		119.4
Used	540.5	516.5		119.4
Sb5V1W0.5–Al				
Fresh	540.2	516.2	245.9	119.4
Used	540.5	517.0	247.5	119.4
Sb5V1W1–Al				
Fresh	540.1	516.5	247.3	119.4
Used	540.7	516.6	247.6	119.4
Sb5V1W2–Al				
Fresh	540.3	516.9	247.1	119.4
Used	540.3	516.0	247.0	119.4
Sb5V1W5–Al				
Fresh	540.7	516.9	247.9	119.4
Used	540.8	516.2	247.4	119.4
WO_3			247.7	
Sb_2O_4/Sb_2O_5	539.9/540.3			
γ-Al_2O_3				119.4
V_2O_5/VO_2		517.1/516.1		

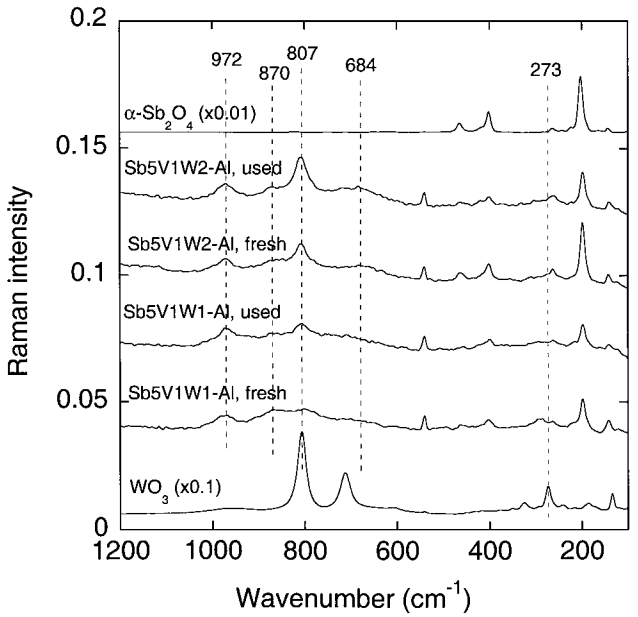

FIG. 6. Raman spectra of WO_3, α-Sb_2O_4, and of Sb5V1W1–Al and Sb5V1W2–Al before and after use in propane ammoxidation. The small peak at 540 cm^{-1} is an instrumental artefact peak, which can be used for quantitative comparisons.

a small peak at 807 cm^{-1} and an even smaller one around 720 cm^{-1}. All bands decrease in intensity after use of the sample in propane ammoxidation.

Transmission electron microscopy. The Sb5V1W1–Al sample was chosen as representative for the Al–Sb–V–W–O catalysts and was characterized using transmission electron microscopy. The investigation indicated the presence in the sample of crystalline antimony oxide in the form of α-Sb_2O_4, which appeared as relatively large crystals with an uneven surface; cf. Fig. 8.

Tungsten oxide WO_3 occurred in crystals which were of similar size as those of α-Sb_2O_4, but the former crystals exhibited an approximately rectangular shape, Fig. 9c. The crystal structure of monoclinic and triclinic WO_3 consists of distorted versions of the ReO_3-type of structure, which is cubic with the lattice constant $a = 3.7$ Å (23). The strong reflections corresponding to this basic structure are prominent in the diffraction patterns in Figs. 9a and 9b, where the diffractograms have been indexed on the basic unit cell. Inspection of the diffraction patterns reveals a set of extra spots, which require a doubling of the unit cell size ($2 \times 3.7 = 7.4$ Å) in the three orthogonal directions. This result fits well for monoclinic WO_3, since this phase exhibits a unit cell with the dimensions $a = 7.30$ Å, $b = 7.54$ Å, $c = 7.69$ Å, $\alpha = \gamma = 90°$, and $\beta = 90.9°$ (24).

Moreover, a phase of rutile-type was observed as aggregates consisting of nanometer-sized crystals, Fig. 10. The aggregates were sometimes found together with crystals of α-Sb_2O_4 or WO_3; see Fig. 8a. When the electron beam was focused on an aggregate of rutile-type crystals, like the one in Fig. 10a, a ring pattern typical for rutiles was observed in diffraction mode, Fig. 10b. This observation indicates that the crystals in the aggregate were randomly oriented, which was confirmed by imaging at high magnification; see Fig. 10c. From the diameter of the rings, the approximate tetragonal lattice parameters were determined to be $a = b = 4.7$ Å and $c = 3.1$ Å. These parameters compare rather well with the basic unit cell determined for the phase $Sb_{0.9}V_{0.9}O_4$, i.e., $a = b = 4.63$ Å and $c = 3.03$ Å (18).

Alumina was observed in the form of aggregates consisting of oriented nanocrystals, which gave single-crystal-type diffraction patterns indicating the presence of δ-Al_2O_3, Fig. 11. This alumina polymorph has a spinel-related crystal structure (25). Similar aggregates of δ-Al_2O_3 were also observed in the Al–Sb–V–O system (16).

Comparison of the Sb5V1W1–Al before and after use in propane ammoxidation showed the presence of the same phases. However, the aggregates of rutile-type crystals appeared much more frequently in the used sample and were rather difficult to observe in the freshly prepared sample.

X-ray microanalysis. Elemental analysis of the rutile-type phase in the Sb5V1W1–Al sample was undertaken in a transmission electron microscope using X-ray microanalysis. Before analysis was performed, aggregates of the rutile-type phase were first identified by their ring pattern in selected area electron diffraction mode. An attempt was then made to analyse a single crystallite at the edge of the aggregate facing the detector. The results of the analyses are presented in Fig. 12 for the freshly prepared sample, and in

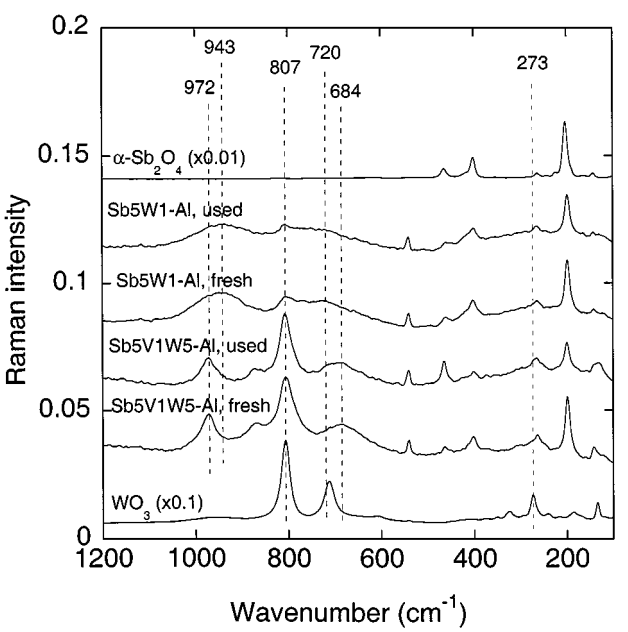

FIG. 7. Raman spectra of Sb5V1W5–Al and Sb5W1–Al before and after use in propane ammoxidation together with the spectra of α-Sb_2O_4 and WO_3. The small peak at 540 cm^{-1} is an instrumental artefact peak, which can be used for quantitative comparisons.

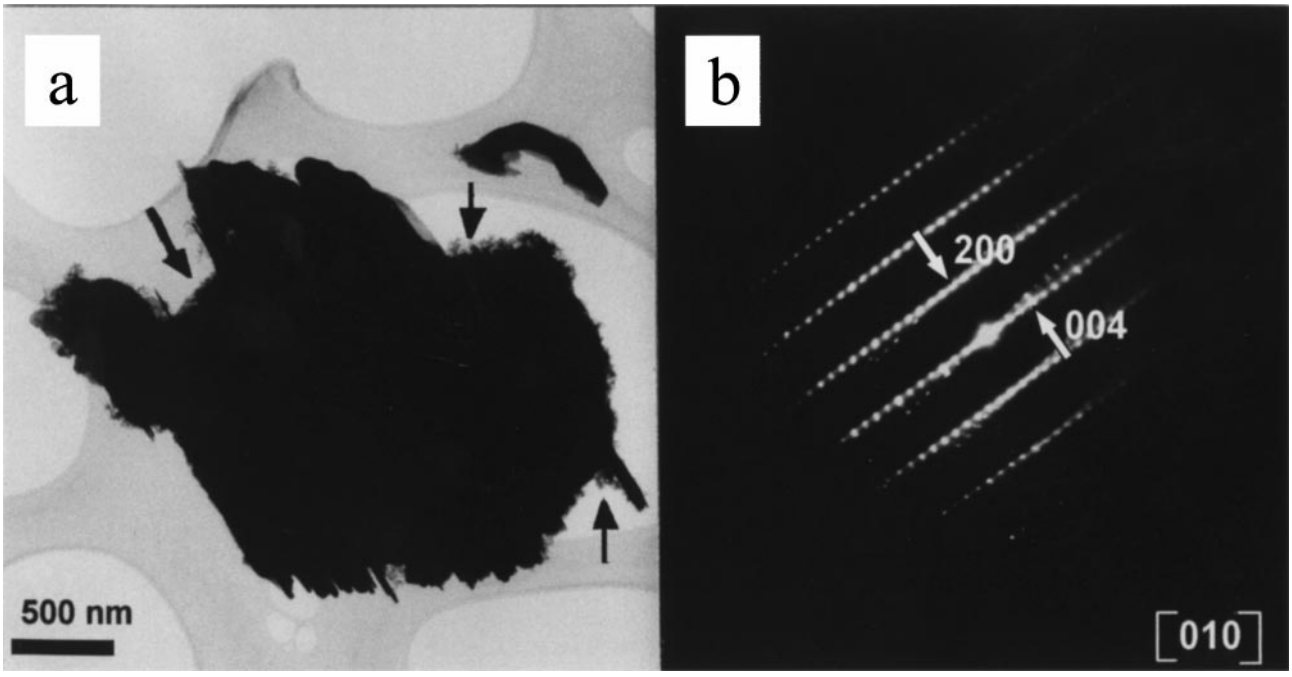

FIG. 8. (a) Transmission electron micrograph of an α-Sb_2O_4 crystal with nanocrystalline aggregates of rutile-type Sb(V, W)O_4 on the surface (arrowed). (b) Electron diffraction pattern of α-Sb_2O_4 taken along the [0 1 0] axis of the crystal. The pattern is indexed using the orthorhombic unit cell with $a = 5.43$ Å, $b = 4.79$ Å, and $c = 11.73$ Å.

Fig. 13 for the sample after use in ammoxidation. Since the analyses usually gave a low and varying aluminum content (Figs. 12a and 13a) and considering that the nominal alumina content in Sb5V1W1–Al was 50 wt%, the analyses possibly include a contribution from the alumina support to the Al-signal. Therefore, the metal content excluding the aluminum is shown in Figs. 12b and 13b. Comparison of Figs. 12 and 13 shows that the calculated antimony content is higher for the freshly prepared sample than for the sample after it has been used in propane ammoxidation. For both samples, generally the analyses show that the V/W atomic ratio in the rutile-type crystals varies in the range 0.5–2.

DISCUSSION

The Alumina Surface

The Raman spectrum in Fig. 5 of α-Sb_2O_4 shows bands at 464, 402, 262, 202, and 142 cm^{-1}, in agreement with previous reports (15, 26). In the Raman spectrum of the freshly prepared Sb5V1–Al in Fig. 5, besides bands from α-Sb_2O_4, there is a weak band at 870 cm^{-1}. The latter band is characteristic of oxidized $\approx SbVO_4$ (14, 15), and the almost absence of this band in the corresponding spectrum after use in propane ammoxidation reveals either reduction forming the reduced $Sb_{1.1}V_{0.9}O_4$ (15), or reaction with Al forming another phase. In a previous comprehensive investigation (16) we have shown that the Sb5V1–Al sample, besides δ-Al_2O_3, consists mainly of (Al, V)SbO_4, which is a rutile-related phase with the composition $Al_{1-x}SbV_xO_4$, $0 < x < 0.5$. As the Raman spectrum of Sb5V1–Al in Fig. 5 shows, (Al, V)SbO_4 gives no bands in Raman.

The Raman spectra of the fresh and the used Sb5V1W0.5–Al sample are very simlar to the corresponding spectra for Sb5V1–Al. Considering the fact that the WO_3 content in Sb5V1W0.5–Al corresponds to 5.4 wt%, the absence of Raman bands from WO_3 in the spectrum of Sb5V1W0.5–Al and the fact that no XRD lines from WO_3 was observed (Table 2) can be explained by the formation of the rutile-type structure (Fig. 10) with W (Figs. 12 and 13), which is X-ray amorphous and apparently inactive in Raman.

The Raman spectra of Sb5V1W1–Al and Sb5V1W2–Al in Fig. 6 and the the spectra of Sb5V1W5–Al in Fig. 7, besides the bands from α-Sb_2O_4, show additional bands at 972, 870, 807, and 684 cm^{-1}. The latter bands grow in intensity when the tungsten content is increased. Comparison with Raman spectra in the literature of alumina supported tungsten oxide admits the two bands at 972 and 870 cm^{-1} to be assigned to a tetrahedral WO_4 species being attached to the alumina surface (27–29). The bands at 807 and 684 cm^{-1} are not from crystalline WO_3, which presents two intense bands at 807 and 712 cm^{-1} (see Fig. 6). Both monoclinic and triclinic WO_3, which were identified in the samples using XRD (Table 2), have been reported to give Raman bands at the two latter positions (30). Usually these bands have

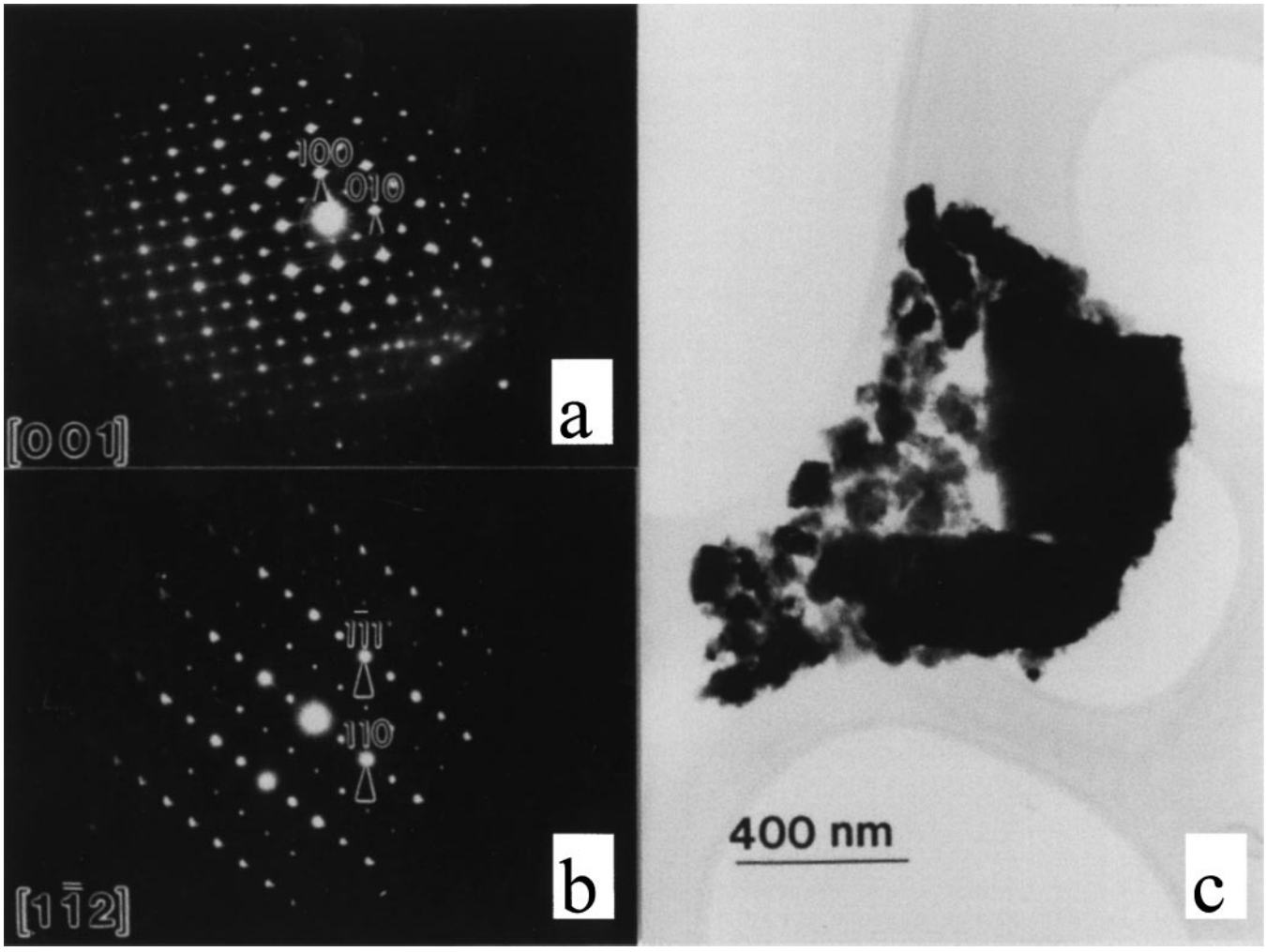

FIG. 9. (a) Electron diffraction of a WO_3 crystal with the [0 0 1] axis parallel to the electron beam. (b) WO_3 crystal with the [1 –1 2] axis along the beam. The diffraction patterns of WO_3 are indexed using a basic ReO_3-type unit cell with $a = b = c = 3.7$ Å. (c) Transmission electron micrograph of WO_3 crystals.

been observed for WO_3/Al_2O_3 samples which have been prepared with high loading of tungsten oxide (27) or at high calcination temperature (31). The monoclinic and triclinic polymorphic forms of WO_3 can be described as constructed from WO_6 octahedra linked by corner sharing (32). There also exists a hexagonal form of WO_3 (33), which is built up of WO_6 octahedra, sharing their corners arranged in six-membered rings. This phase gives Raman bands at 817 and 690 cm^{-1} (34). In the light of the positions of Raman bands for the various WO_3 polymorphs, we propose that the two Raman bands at 807 and 684 cm^{-1} in the spectra of the Al–Sb–V–W–oxide samples in Figs. 6 and 7 can be assigned to an octahedral WO_6 species being attached to the alumina surface. The fact that these bands are observed in the current work but have not been reported in the previous characterizations of WO_3/Al_2O_3 samples (27–29) could be due to the doping of the alumina with vanadium and/or antimony. Considering that XRD showed only a few lines from crystalline WO_3 and Raman spectroscopy revealed no other structure with tungsten than the tetrahedral and octahedral surface species on the alumina, it is of interest to notice that the content of tungsten oxide in Sb5V1W5–Al, 27.4 wt%, corresponds to approximately two theoretical monolayers defining a monolayer as 4×10^{18} W atoms/m^2 (31). These facts are consistent with the phase of rutile-type with tungsten being present in the samples.

Both the freshly prepared and the used Sb5W1–Al show in Fig. 7 Raman features which are different from those of the samples containing vanadium. Sb5W1–Al gives a broad band at 943 cm^{-1}, which possibly stems from a tetrahedral WO_4 species with water ligands (28). Another band appears at 807 cm^{-1} and there is also a very weak feature around 720 cm^{-1}, both of which possibly could be from crystalline WO_3.

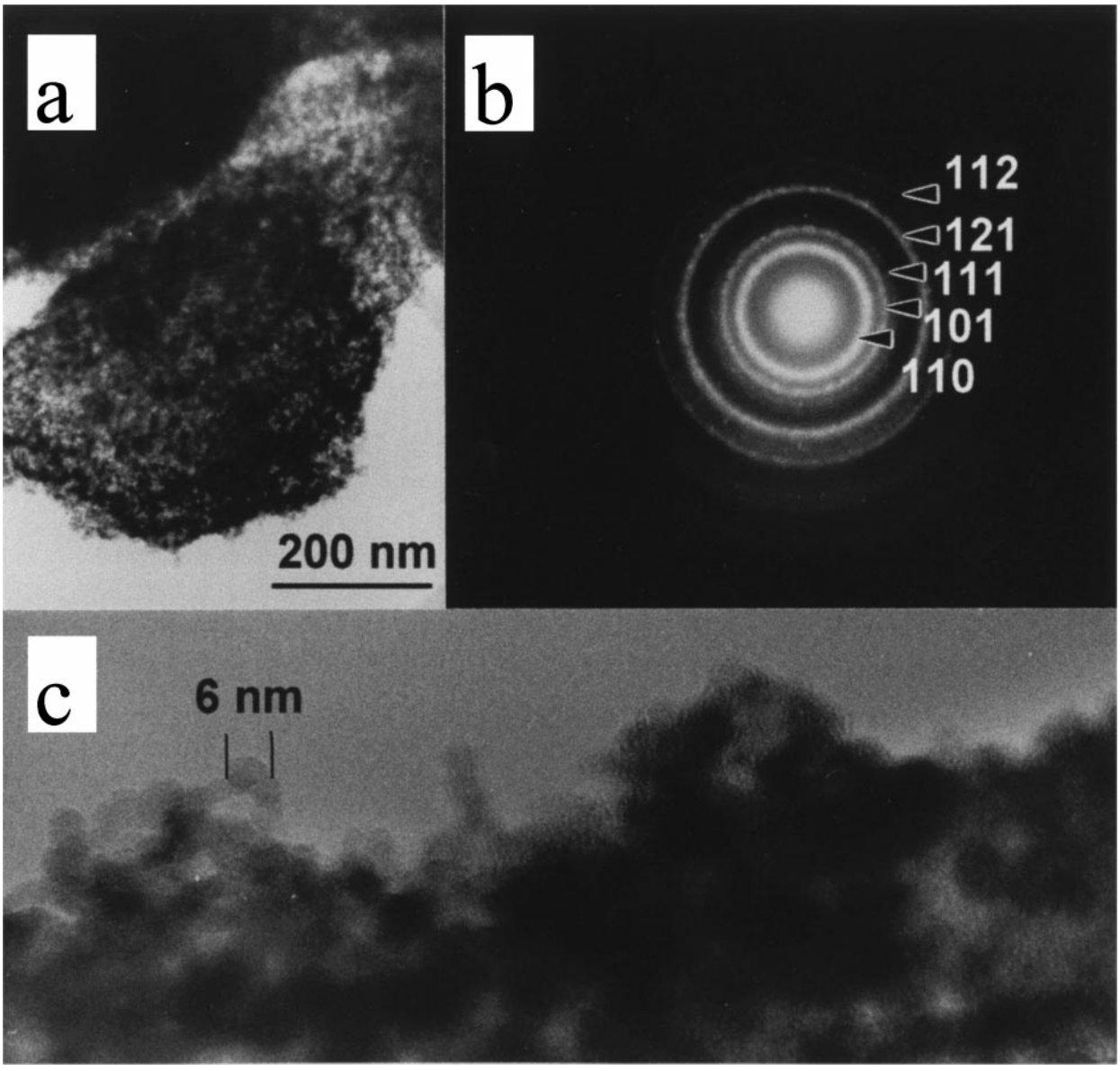

FIG. 10. Rutile-type $\approx$Sb(V, W)O_4. (a) Transmission electron micrograph of an aggregate consisting of nanocrystals. (b) Electron diffraction pattern from the aggregate, which is indexed on the tetragonal unit cell with $a = b = 4.7$ Å and $c = 3.1$ Å. (c) High-magnification image showing randomly oriented nanocrystals of $\approx$Sb(V, W)O_4.

Composition of the Active Rutile Phase

Investigation of Sb5V1W1–Al before and after use in propane ammoxidation with electron microscopy and electron diffraction (ED) as well as with XRD shows the presence of δ-Al_2O_3 (ED), α-Sb_2O_4 (XRD, ED), WO_3 (XRD, ED), and a phase of rutile-type (ED). Elemental analysis of the latter phase shows signals from Sb, V, W, and Al. However, the results in Figs. 12a and 13a show a scattered Al-content, which is in support of the rutile phase itself being without aluminum and the Al-signal being from the alumina support (50 wt%). Figure 10 reveals that the rutile is present in the form of polycrystalline aggregates, consisting of very small crystallites which are less than 10 nm in diameter. An important observation was that the freshly prepared sample, compared with the used one, was much less homogeneous and the polycrystalline aggregates of the rutile phase appeared considerably less frequent. The elemental analyses excluding the aluminum, which are presented in Fig. 13b, show that the composition of the crystals of rutile-type varies in the range $Sb_{0.9}V_{0.9-x}W_xO_4$, where $0.3 < x < 0.6$, and is on average $Sb(V)_{0.9}V(III, IV)_{0.45}W(IV)_{0.45}O_4$ after activation of the sample in propane ammoxidation. The reason for the variation can be that heating above the

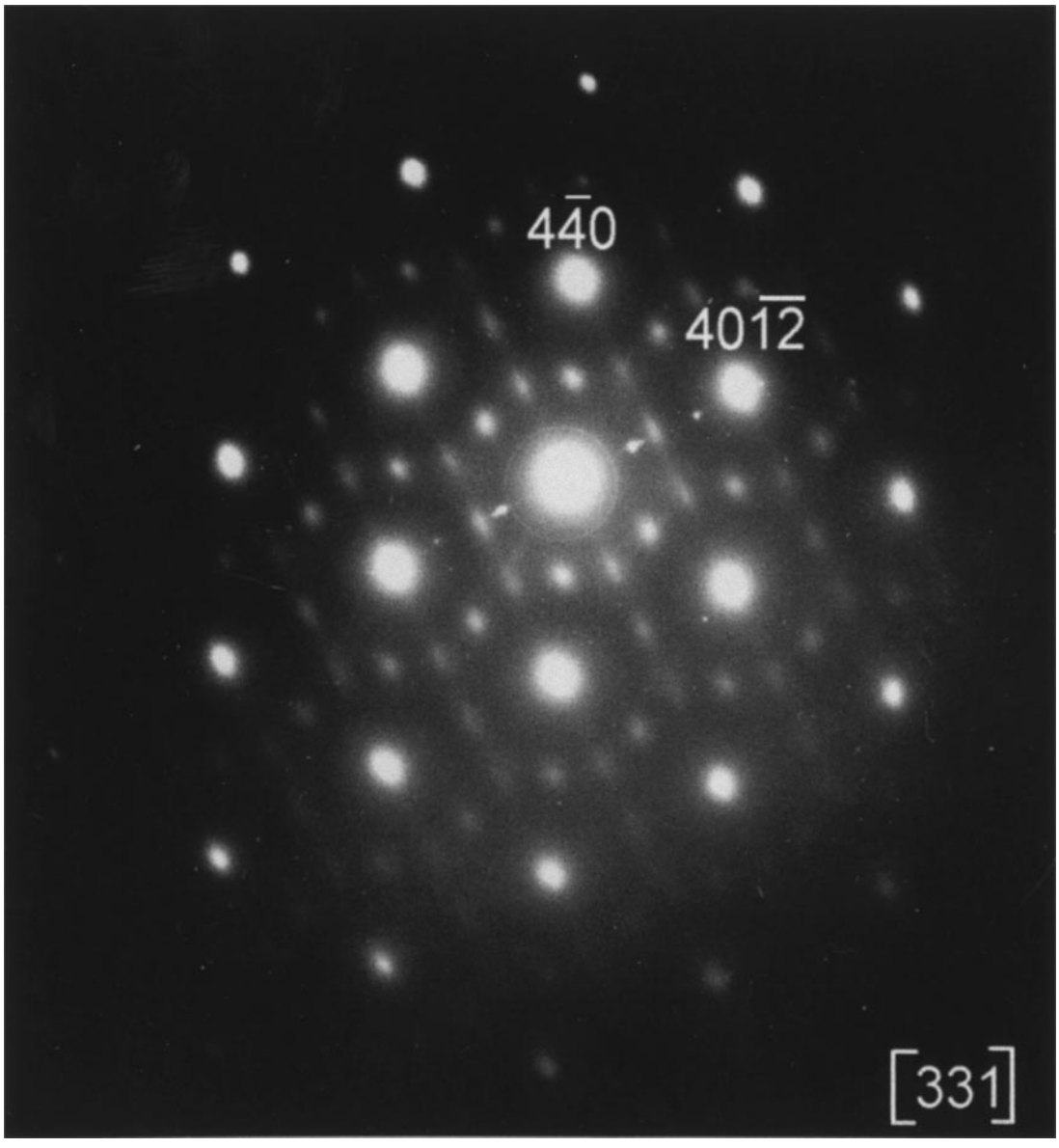

FIG. 11. Electron diffraction pattern of δ-Al_2O_3 recorded with the beam along the [3 3 1] direction in the highly oriented crystallites. The indices refer to the tetragonal unit cell with $a = b = 7.94$ Å and $c = 23.50$ Å.

calcination temperature (610°C) is required for obtaining a homogeneous composition. Although only Sb5V1W1–Al with the atomic ratio V/W = 1 was subjected to comprehensive analysis, the range of the analysis results indicates that the corresponding rutile crystals in Sb5V1W0.5–Al should be less rich in tungsten and have the average composition $Sb_{0.9}V_{0.6}W_{0.3}O_4$, while in Sb5V1W2–Al the average composition should be $Sb_{0.9}V_{0.3}W_{0.6}O_4$. In Sb5V1W5, possibly rutile crystals even richer in tungsten can form. It is of interest to notice that unlike what we have observed for the Al–Sb–V–oxide system (16), we have found no evidence in the current work for the formation of the (Al, V)SbO_4 rutile phase. Considering the Raman spectroscopic results in Figs. 6 and 7, an explanation for (Al, V)SbO_4 not being formed when tungsten is present can be that coverage of the alumina surface with WO_4 and WO_6 surface species hinders the alumina from reacting with Sb- and V-oxide. Instead the latter oxides react with tungsten oxide forming $Sb_{0.9}V_{0.9-x}W_xO_4$, which can be considered to be a solid solution between the $Sb_{0.9}V_{0.9}\square_{0.2}O_4$ phase having cation vacancies □ (18, 19) and WO_2. Substitution of V^{4+} with W^{4+} agrees with the slight enlargement of the unit cell that was observed. In a previous work (17) we reported formation of $Al_{0.1}Sb_{0.8}V_{0.7}W_{0.4}O_4$, which was described as a solid solution between (Al, V)SbO_4 and WO_2. However, the analyses in the current work should be more accurate, since the

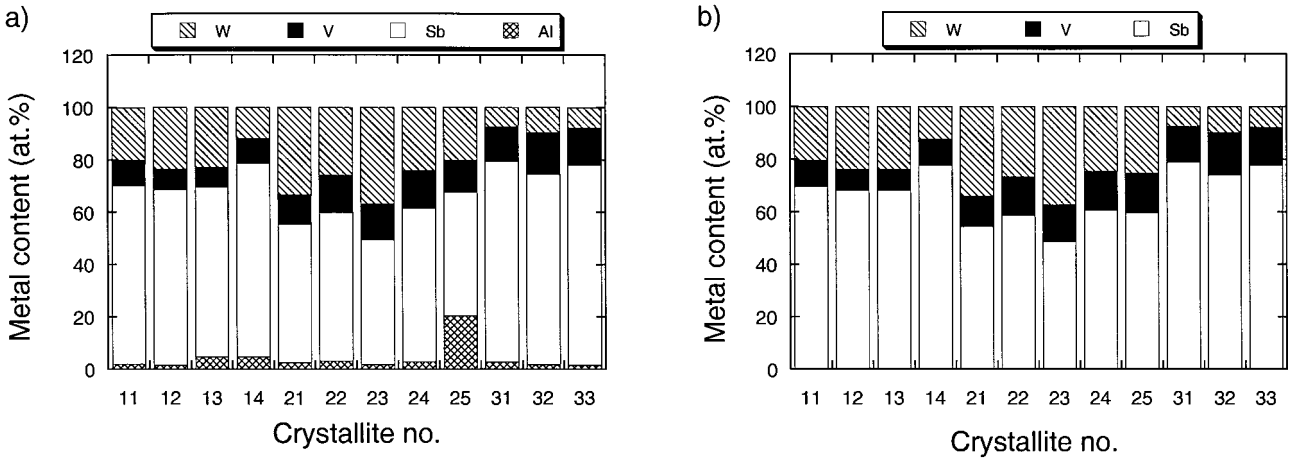

FIG. 12. X-ray microanalysis of the aggregated rutile-type crystallites in freshly prepared Sb5V1W1–Al. (a) Metal content in at% and (b) metal content in at% after the contribution from aluminum has been excluded. In the crystallite numbers given in the figure, the first digit is the aggregate number and the second digit is the number of the crystallite in the aggregate.

composition of the rutile crystals was determined using a smaller beam diameter, 1 nm instead of 50 nm, and also a larger number of crystals were analyzed.

Quantitative XPS data in Table 3, showing that the Al-content at the surface is considerably lower than the nominal value, are in support of the alumina surface being covered with oxides containing Sb, V, and W. For the used Sb5V1W2 and Sb5V1W5 samples, the atomic Sb/(V + W) surface ratio according to XPS is around 1 and of similar magnitude for the used Sb5V1W1, which agrees with the ratio in $Sb_{0.9}V_{0.9-x}W_xO_4$. Regarding the V/W ratio, the XPS analyses show no clear trend with the variation of the nominal W-content of the catalysts, which can be due to the fact that XPS gives information from several mm^2 of the surface to be compared with EDX analysis giving information from almost one single crystal (nm-scale).

Activation Processes

The activation behaviour that was observed for the catalysts with tungsten, and which is exemplified in Fig. 1 for Sb5V1W2–Al, reasonably is related to a phase containing vanadium, since Fig. 2 shows a clear correlation between catalytic activity and the vanadium content of the catalyst. Previously we have reported the same relationship (16, 20). Two activation processes can be distinguished, namely a long-term activation of the freshly prepared catalyst, extending over 15–50 h depending on the W-content, as well as a short-term reactivation after close down of the reactor overnight. The long-term activation behaviour, see Fig. 1 and Ref. (17), shows up as an increase in activity together with a considerable increase in the selectivity to acrylonitrile, which primarily is coupled to a decrease in the

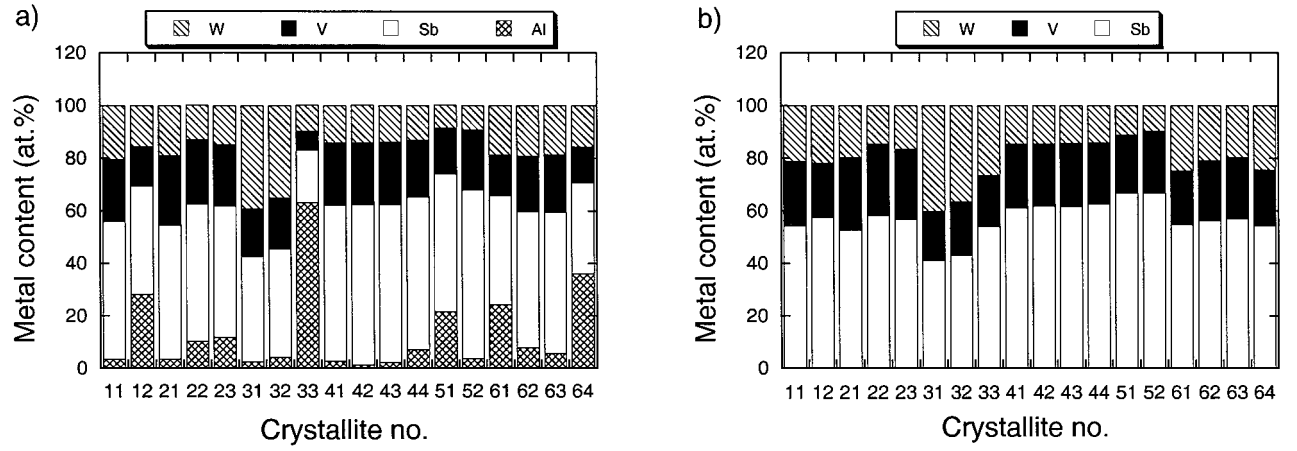

FIG. 13. X-ray microanalysis of the aggregated rutile-type crystallites in Sb5V1W1–Al after use of the sample in propane ammoxidation. (a) Metal content in at% and (b) metal content in at% after the contribution from aluminum has been excluded. In the crystallite numbers given in the figure, the first digit is the aggregate number and the second digit is the number of the crystallite in the aggregate.

formation of waste products. On the other hand, the short-term reactivation is apparent as an increase in total activity and selectivity to acrylonitrile, while there is a concurrent decrease of the selectivity to propylene. Apparently, there may be different explanations for the two activation processes.

Concerning the long-term activation, this process is not primarily related to spreading of active phase over the alumina surface, since the quantitative XPS results in Table 3 rather show some increase in the Al-content at the catalyst surface after it has been used in propane ammoxidation. Since this activation process lasts for a period up to a few days, it is possibly not caused solely by a reconstruction of the surface, but rather it concerns the bulk material of the catalyst. The microscopy work revealed that the polycrystalline aggregates of the $Sb_{0.9}V_{0.9-x}W_xO_4$ rutile phase were more frequent in occurrence after than before use of the sample in the ammoxidation. Thus, the long-term activation behaviour can be related to the formation of active and selective $\approx$Sb(V, W)O_4 from a nonselective catalyst precursor with low activity and which, besides δ-Al_2O_3, WO_3, α-Sb_2O_4, WO_3/Al_2O_3, and possibly some $\approx SbVO_4$ (Fig. 5), consists of an inhomogeneous and not very crystalline material. According to the XPS analyses in Table 3 and the EDX data in Fig. 12, the external layers of the catalyst precursor are rich in antimony. This result indicates either spreading of surplus antimony oxide over the freshly prepared surfaces or enrichment of Sb at the surfaces of the precursor material. Formation of more of the active rutile phase during the long-term activation process explains the finding that the intensity of the Raman bands from α-Sb_2O_4 is lower after use in ammoxidation than it is before use (cf. Figs. 5–7). In agreement with this observation are the XPS data in Table 3, showing that upon use in ammoxidation of the samples with tungsten there is an increase at the surface of the V and W content, which is associated with a decrease of the Sb content. The fact that the catalytic reaction promotes the formation of the rutile phase with tungsten primarily can be due to the fact that under influence from the reaction medium W^{6+} is reduced to W^{4+}, which can accommodate in a structure of rutile-type. Reduction of vanadium and antimony, of course, can also occur (14, 15). However, this is possibly not the main cause of the long-term activation process, since $\approx SbVO_4$ with Sb^{5+} and V^{3+}/V^{4+} is a bad catalyst (cf. Fig. 2) and is easily obtained during calcination in air of preparations without tungsten (15). Thus, the evolution shown in Fig. 1 can be explained; i.e., the activity increases due to increase of the surface content of active vanadia species. The concurrent increase of the selectivity to acrylonitrile, then, can be seen as a result of tuning of the active ensemble by incorporation of tungsten in the rutile structure. The present results indicate that crystallization of the precursor material improves the catalytic performance, as opposed to a previous report where it was indicated that formation of more crystalline systems gives worse catalytic behaviour (10). However, the multiphase Al–Sb–V–W–oxide system is complex and the contradiction in conclusion here is most likely due to differences in the catalyst synthesis.

The short-term activation process hardly concerns the changes in the structure of the bulk materials, but more likely is due to a relatively faster restructuring of the catalyst surface and external layers. It is possible that this activation is related to partial reduction of the catalyst, since when restarting the reactor the catalyst was heated to the reaction temperature in air. Another possiblity is that the activation is connected with a change in the Sb : V : W surface ratio under influence from the temperature and the atmosphere, since it is known that in oxides with more than one metal their ratio at the surface depends on the atmosphere (35).

The binding energies measured by XPS (Table 4) for Sb $3d_{3/2}$, V $2p_{3/2}$, and W $4d_{5/2}$ show no significant differences between the freshly prepared samples and those being used in propane ammoxidation. A complication in this regard is that some of the surface species that were reduced in the catalytic reaction may partially reoxidise during transfer of the sample from the reactor to the spectrometer. On the other hand, some species may be reduced under influence of the vacuum in the spectrometer. These considerations give rise to some uncertainty in correlating oxidation states to the measured binding energies for the fresh and reactive phases. The Sb $3d_{3/2}$ binding energy for the pure α-Sb_2O_4 was measured to be 539.9 eV, while the corresponding values for the catalysts and their precursors are 540.1–540.8 eV, indicating the presence of Sb^{5+} states at the surface (14, 15, 36). However, a contribution from Sb^{3+} states to the Sb $3d_{3/2}$ signal cannot be ruled out, since the difference in binding energy between Sb^{3+} and Sb^{5+} is within 0.8 eV (36). For vanadium the V $2p_{3/2}$ binding energy values in Table 4 are around 516.5 ± 0.5 eV in precursors and catalysts, indicating the presence of V^{4+} and V^{5+} states at the surfaces (37). For crystalline WO_3 the measured binding energy for W $4d_{5/2}$ is 247.7 eV. A shift of the order of 1 eV towards lower binding energy can be expected for WO_2 (38). The data in Table 4 for the W $4d_{5/2}$ binding energies of the precursors and activated samples show some scattering, but they are usually somewhat lower than the value for WO_3. The magnitude of the shift indicates the presence of both W^{6+} and W^{5+} or W^{4+} states at the surfaces of the precursors and the catalysts. Contribution to the W^{6+} states comes primarily not from WO_3, since it is present in small amount, but rather from the tetrahedral WO_4 and octahedral WO_6 species on the alumina surface. It has been reported that alumina stabilizes tungsten oxide surface species as W^{6+} (38). Contribution to the W $4d_{5/2}$ signal from W^{4+}, as well as the appearance of Sb^{5+} and V^{4+} oxidation states, agrees with the formation of a $Sb_{0.9}V_{0.9-x}\square_{0.2}W_xO_4$ rutile phase with cation vacancies ($\square$) and in which the valence states of Sb, V, and W in the

bulk are 5+, 4+, and 4+, respectively. Chemical analysis of the vanadium in an Al–Sb–V–W–oxide catalyst showed in addition to V^{4+} the presence of about 10% as V^{3+} after use of the sample in propane ammoxidation (39). This finding is not contradictory to the formula for the rutile phase, since V^{4+} in the structure can be reduced to V^{3+} in parallel with filling of the cation vacancies and segregation of antimony and tungsten oxide (18).

Comparison of the Sb–V–O, Al–Sb–V–O, and Al–Sb–V–W–O Systems

The activity data in Fig. 2 show that the pure $\approx SbVO_4$ phase is unselective towards the formation of acrylonitrile, an observation which is in agreement with previous reports (9, 14–17, 20). Comparison of the data for Sb2V1 with those for $\approx SbVO_4$ shows that there is considerable increase in the selectivity to acrylonitrile when antimony is present in excess (Sb/V > 1) of the amount required for forming $\approx SbVO_4$. Moreover, Figs. 2 and 4 show that the selectivity and the yield both towards the intermediate product propylene and to acrylonitrile increase when aluminum (Sb5V1–Al) is added to the system. There is also substantial improvement in the catalytic data when W is added (Sb5V1W1–Al, Sb5V1W2–Al). The successive improvement of the catalytic properties for propane ammoxidation with addition to $\approx SbVO_4$ of excess Sb, Al, and W is in line with data given in patents (8) and the literature (9, 10, 17, 39). At first sight, it may seem that Sb and Al additions play the same role in each of the three systems Sb–V–O, Al–Sb–V–O, and Al–Sb–V–W–O. However, this is not the case and there are important differences. Considering the literature, two roles of the excess antimony oxide (Sb/V > 1) can be distinguished in the Sb–V–O system, namely, (i) for the formation of suprasurface antimony sites, creating isolation of V-sites to a suitable degree at the surface (14–17, 20) and (ii) for completing the reaction between antimony and vanadium oxide (36). The effect is apparent as increase in the selectivity and the yield to acrylonitrile due to less formation of carbon oxides and less degradation of ammonia to nitrogen. On the other hand, in the Al–Sb–V–O system the active phase has been identified to be a trirutile-like phase with the compostion $Al_{1-x}SbV_xO_4$, where $0 < x < 0.5$ (16). Moreover, the presence in the synthesis of an excess of aluminum was found to be critical for its formation. Thus, the Sb/V ratio is greater than one in the bulk of the rutile phase and the aluminum in this system is not only a catalyst support in form of Al_2O_3 but is also an element in the active phase. In the current work on the Al–Sb–V–W–O system we have identified formation of a rutile phase with the composition $Sb_{0.9}V_{0.9-x}W_xO_4$ as being active and selective for propane ammoxidation. Also in this case is the atomic Sb/V ratio in the bulk of the rutile larger than one, but the alumina acts primarily as a catalyst support.

Considering the results as they have appeared for propane ammoxidation on the Sb–V–O, Al–Sb–V–O, and Al–Sb–V–W–O systems, it is apparent that the data can be rationalized in terms of the site isolation theory. This theory, which was orginally formulated by Callahan and Grasselli (40), has previously been used as a basis in the development of oxide catalysts for propylene ammoxidation (41). In the three systems for propane ammoxidation, vanadium is a cardinal element for the activation of propane. However, since ensembles with too many vanadium atoms give waste products (16, 36), it is necessary to create structural isolation of the V centers. Isolation is thus obtained by surrounding the vanadium moieties with Sb (Sb–V–O), Sb and Al (Al–Sb–V–O), or Sb and W (Al–Sb–V–W–O). The present data for the Al–Sb–V–W–oxide system, showing a yield to acrylonitrile of 37% at almost 80% propane conversion, are in agreement with the data given in patents for similar reaction conditions (8). Further improvement of the properties of the Al–Sb–V–W–oxide system possibly can be achieved by promotion with other elements. It has been reported that the addition of Te and Sn to the catalyst gives some improvement (8, 42), and recently, it has been reported that enhanced selectivity of the catalyst is obtained by vapour-phase deposition of silane followed by oxidation (43).

CONCLUSIONS

Al–Sb–V–W–oxide catalyst precursors, which have been calcined in air at 610°C, show in propane ammoxidation at 480°C an activation behaviour which extends up to a few days. Under influence from the reaction medium a catalyst structure is formed, which is active and selective to acrylonitrile formation.

Characterization of the catalyst and the precursor material with high-resolution electron microscopy, electron diffraction, and X-ray microanalysis reveals the presence of a rutile-type phase, the formation of which is enhanced under influence from the reaction medium. According to X-ray microanalysis, the composition of the phase is $Sb_{0.9}V_{0.9-x}W_xO_4$, $0.3 < x < 0.6$, which can be considered to be a solid solution between $Sb_{0.9}V_{0.9}O_4$ and WO_2. XPS measurements show that the content of Sb at the surface decreases during the activation of the precursor material, while the V and W contents increase. The increase of the vanadium content explains the increase in propane conversion with time-on-stream during the activation period. The concurrent increase of the selectivity to acrylonitrile formation can be seen as a consequence of incorporation of W^{4+} into the rutile-type structure, tuning the catalytic performance of the active ensemble.

Raman spectroscopy gives information about the alumina surface, showing the presence of tetrahedral and octahedral tungsten oxide species attached to the alumina.

The alumina is a catalyst support, and no evidence for the formation of (Al, V)SbO_4 (16) was obtained.

Compared with Sb–V–oxide and Al–Sb–V–oxide preparations, the Al–Sb–V–W–oxide system gives enhanced catalytic properties. Over a catalyst with the atomic ratio Sb : V : W = 5 : 1 : 2 on alumina (50 wt%), the yield to acrylonitrile is 37% at 77% propane conversion. The results collected for the Al–Sb–V–W–oxide system and the subsystems can be rationalized in terms of the site isolation theory (40, 41). Isolation of active vanadia moieties in the structure, through the incorporation of Sb and Al or W, is a key factor for obtaining a selective catalyst.

ACKNOWLEDGMENTS

Financial support from the Swedish National Research Council for Engineering Sciences (TFR), the Swedish Natural Science Research Council (NFR), and the Ministerio Español de Educación y Ciencia is gratefully acknowledged.

REFERENCES

1. Wittcoff, H. A., *CHEMTEC* **20**, 48 (1990).
2. Malow, M., *in* "Handbook of Chemicals Production Processes" (R. A. Meyers, Ed.), Ch. 1.9. McGraw–Hill, New York, 1986.
3. Newsletter, *Appl. Catal.* **67**, N5 (1990).
4. BP Amoco, http://www.bpamoco.com, press release, 29 May, 1997.
5. U.S. Patents 4,760,154 (1988), 4,835,125 (1989), 4,837,191 (1989), and 4,843,055 (1989), assigned to the Standard Oil Company (Ohio).
6. Kim, Y.-C., Ueda, W., and Moro-oka, Y., *Appl. Catal.* **70**, 189 (1991).
7. Kim, Y.-C., Ueda, W., and Moro-oka, Y., *in* "New Developments in Selective Oxidation" (G. Centi and F. Trifirò, Eds.), Studies in Surface Science and Catalysis, Vol. 55, p. 491. Elsevier, Amsterdam, 1990.
8. U.S. Patents 4,746,641 (1988), 4,788,317 (1988), assigned to the Standard Oil Company (Ohio).
9. Centi, G., Grasselli, R. K., Patanè, E., and Trifirò, F., *in* "New Developments in Selective Oxidation" (G. Centi and F. Trifirò, Eds.), Studies in Surface Science and Catalysis, Vol. 55, p. 515. Elsevier, Amsterdam, 1990.
10. Centi, G., Trifirò, F., and Grasselli, R. K., *Chim. Ind. (Milan)* **72**, 617 (1990).
11. Ushikubo, T., Oshima, K., Kayou, A., Vaarkamp, M., and Hatano, M., *J. Catal.* **169**, 394 (1997).
12. Birchall, T., and Sleight, A. W., *Inorg. Chem.* **15**, 868 (1976).
13. Berry, F. J., Brett, M. E., and Patterson, W. R., *J. Chem. Soc. Dalton Trans.*, 9 (1983).
14. Nilsson, R., Lindblad, T., Andersson, A., Song, C., and Hansen, S., *in* "New Developments in Selective Oxidation II" (V. Cortéz Corberán, and S. Vic Bellón, Eds.), Studies in Surface Science and Catalysis, Vol. 82, p. 293. Elsevier, Amsterdam, 1994.
15. Nilsson, R., Lindblad, T., and Andersson, A., *J. Catal.* **148**, 501 (1994).
16. Nilsson, J., Landa-Cánovas, A. R., Hansen, S., and Andersson, A., *J. Catal.* **160**, 244 (1996).
17. Nilsson, J., Landa-Cánovas, A. R., Hansen, S., and Andersson, A., *in* "Proceedings, 3rd World Congress on Oxidation Catalysis, San Diego, 1997" (R. K. Grasselli, S. T. Oyama, A. M. Gaffney, and J. E. Lyons, Eds.), Studies in Surface Science and Catalysis, Vol. 110, p. 413. Elsevier, Amsterdam, 1997.
18. Landa-Cánovas, A., Nilsson, J., Hansen, S., Ståhl, K., and Andersson, A., *J. Solid State Chem.* **116**, 369 (1995).
19. Hansen, S., Ståhl, K., Nilsson, R., and Andersson, A., *J. Solid State Chem.* **102**, 340 (1993).
20. Nilsson, J., Landa-Cánovas, A., Hansen, S., and Andersson, A., *Catal. Today* **33**, 97 (1997).
21. Catani, R., Centi, G., Trifirò, F., and Grasselli, R. K., *Ind. Eng. Chem. Res.* **31**, 107 (1992).
22. JCPDS International Centre for Diffraction Data, "Powder Diffraction File," Swarthmore, PA, 1991.
23. Yamaguchi, O., Tomihisa, D., Kawabata, H., and Shimizu, K., *J. Am. Ceram. Soc.* **70**, C94 (1987).
24. Loopstra, B. O., and Boldrini, P., *Acta Crystallogr.* **21**, 158 (1966).
25. Lippens, B. C., and de Boer, J. H., *Acta Crystallogr.* **17**, 1312 (1964).
26. Cody, C. A., DiCarlo, L., and Darlington, R. K., *Inorg. Chem.* **18**, 1572 (1979).
27. Salvati, L., Makovsky, L. E., Stencel, J. M., Brown, F. R., and Hercules, D. M., *J. Phys. Chem.* **85**, 3700 (1981).
28. Chan, S. S., Wachs, I. E., Murrell, L. L., Wang, L., and Hall, W. K., *J. Phys. Chem.* **88**, 5831 (1984).
29. Horsley, J. A., Wachs, I. E., Brown, J. M., Via, G. H., and Hardcastle, F. D., *J. Phys. Chem.* **91**, 4014 (1987).
30. Salje, E., *Acta Crystallogr. Sect. A* **31**, 360 (1975).
31. Chan, S. S., Wachs, I. E., Murrell, L. L., and Dispenziere, N. C., *J. Catal.* **92**, 1 (1985).
32. Sundberg, M., *Chem. Commun. Univ. Stockholm* **5** (1981).
33. Gerand, B., Nowogrocki, G., Guenot, J., and Figlarz, M., *J. Solid State Chem.* **29**, 429 (1979).
34. Daniel, M. F., Desbat, B., Lassegues, J. C., Gerand, B., and Figlarz, M., *J. Solid State Chem.* **67**, 235 (1987).
35. Bielanski, A., Camra, J., and Najbar, M., *J. Catal.* **57**, 326 (1979).
36. Andersson, A., Andersson, S. L. T., Centi, G., Grasselli, R. K., Sanati, M., and Trifirò, F., *Appl. Catal. A* **113**, 43 (1994).
37. Andersson, S. L. T., *J. Chem. Soc. Faraday Trans. 1* **75**, 1356 (1979).
38. Wachs, I. E., Chersich, C. C., and Hardenbergh, J. H., *Appl. Catal.* **13**, 335 (1985).
39. Zanthoff, H. W., Schaefer, S., and Wolf, G.-U., *Appl. Catal. A* **164**, 105 (1997).
40. Callahan, J. L., and Grasselli, R. K., *AIChE J.* **9**, 755 (1963).
41. Grasselli, R. K., and Burrington, J. D., *in* "Advances in Catalysis" (D. D. Eley, H. Pines, and P. B. Weisz, Eds.), Vol. 30, p. 133. Academic Press, New York, 1981.
42. Grasselli, R. K., Centi, G., and Trifirò, F., *Appl. Catal.* **57**, 149 (1990).
43. Zanthoff, H. W., Lahmer, M., Baerns, M., Klemm, E., Seitz, M., and Emig, G., *J. Catal.* **172**, 203 (1997).